Weld World (2017) 61:375–381
DOI 10.1007/s40194-016-0415-8

RESEARCH PAPER

Microstructures and mechanical properties of Ti_3Al/Ni-based superalloy joints diffusion bonded with Ni and TiNiNb foils

H. S. Ren [1] · X. Wu [1] · B. Chen [1] · H. P. Xiong [1] · Y. Y. Cheng [1]

Received: 17 September 2016 / Accepted: 15 December 2016 / Published online: 2 January 2017
© International Institute of Welding 2016

Abstract Dissimilar joining of Ti_3Al-based alloy to Ni-based superalloy has been conducted with diffusion bonding method using Ni foil and TiNiNb alloy as interlayer. For the Ni foil, with the increase of bonding temperature, the joint strength increased firstly and then decreased. The joints bonded at 980 °C for 20 min with a pressure of 20 MPa presented the maximum shear strength of 207 MPa at room-temperature. During the bonding process, Ni foil reacted with Ti_3Al-based alloy due to the strong affinity between elements Ti and Ni. The formation of Ni_2Ti, $AlNi_2Ti$, and Ni_3Ti compounds at Ti_3Al/Ni interface limited the mechanical properties of the joint. The use of the TiNiNb alloy decreased the formation tendency of brittle Ti-Ni phases to some extent and only little Ti_2Ni phase was visible in the joint. The shear strength of 209 MPa was obtained under the condition of 980 °C/10 min/20 MPa, close to that obtained through Ni foil. The (Ni,Ti,Nb,Fe,Cr) multi-component phase formed at TiNiNb/GH536 interface became the new weak link of the joint.

Keywords (IIW Thesaurus) Diffusion bonding · Microstructure · Mechanical properties

Recommended for publication by Commission XVII - Brazing, Soldering and Diffusion Bonding

✉ H. P. Xiong
xionghp69@163.com

[1] Welding and Plastic Forming Division, Beijing Institute of Aeronautical Materials, Beijing 100095, China

1 Introduction

Intermetallic compounds have been attracted a great deal of attention, especially when weight reduction and high temperature capability are critical for structural designs [1]. Among these intermetallic alloys, Ti_3Al-based alloy is a potential structural material for aerospace applications due to its relatively low density, high specific strength, excellent creep behavior, and good oxidation stability at elevated temperature [1, 2]. Obviously, to realize its practical application, developing joining technologies of Ti_3Al-based alloy to itself or to other materials such as nickel-based superalloy has become an important issue.

In the past decades, plenty of studies have been made about the joining of Ti_3Al-based alloys, including fusion welding [3–5], linear friction welding [6], brazing [7, 8], and diffusion bonding [9]. Concerning the joining of Ti_3Al-based alloys to themselves, sound joints could be achieved. For example, a Ti_2AlNb-based alloy was welded by linear friction welding (LFW) in Ref. [6], and the tensile strength of the joint was comparable to that of the base metal. Cadden et al. investigated the brazing of Ti–13.4Al–21.2Nb (at.%) alloy using Ti–Cu–Ni system fillers, and the tensile strength of the joint was reached up to 548 MPa [7].

With regard to dissimilar joining, efforts were focused on the joining of Ti_3Al-based alloys to Ti-based alloys. For instance, Tan et al. investigated the electron beam welding of Ti–22Al–25Nb (at.%) to Ti–6.5Al–3.5Mo–1.5Zr–0.3Si (wt.%) alloys [5]. The room-temperature tensile strength of the joint was higher than that of the Ti–6.5Al–3.5Mo–1.5Zr–0.3Si alloy, and the impact toughness value was found to be about 42% of that of the Ti–6.5Al–3.5Mo–1.5Zr–0.3Si alloy. The joining of Ti–22Al–27Nb (at.%) to Ti–6Al–4 V (wt.%) alloys was conducted using laser welding technique, and the average tensile strength of the joints reached about

Table 1 Chemical composition of GH536 superalloy (wt.%)

Cr	Fe	Mo	Co	W	C	Ti	Al	Ni
20.5~23.0	17.0~20.0	8.0~10.0	0.5~2.5	0.2~1.0	0.05~0.15	0.15	0.05	Balance

92% of the Ti–6Al–4 V parent metal [10]. Besides, in Ref. [8], the dissimilar brazing between Ti_3Al-based and Ti–6Al–4 V (wt.%) alloys was carried out and the continuous Ti_2Ni phase deteriorated the joint strength.

Actually, the dissimilar joining of Ti_3Al-based alloy to Ni-based superalloy is more attractive for engineering applications because of its high-temperature service potential as well as the weight reduction effects. However, researches about the joining of these two materials are rarely reported. In a recent paper, an attempt was made to braze a Ti_3Al-based alloy to a Ni-based superalloy using a Ti–Zr–Cu–Ni filler alloy. However, micro-cracks were visible within the dissimilar joint, and the obtained joint shear strength was only 86 MPa [11]. Chen et al. studied the gas tungsten arc (GTA) welding of Ti_3Al-based alloy to In718 superalloy, and the joint tensile strength was 242 MPa [12, 13].

Moreover, Qian et al. investigated the diffusion bonding of Ti–20Al–25Nb (at.%) to In718 superalloy by inserting metal foils of Nb + Ni as interlayer [14]. The joint obtained under the condition of 1050 °C/40 min/20 MPa exhibited a shear strength of 460 MPa. It should be noted that Ni_3Nb and Ni_6Nb_7 compounds were formed, and micropores were visible in both Ti_3Al/Nb and Ni/In718 interfaces. Furthermore, the joint properties at high temperatures were not reported. Therefore, so far, the study on the dissimilar joining of Ti_3Al-based alloy to nickel-based superalloy is still insufficient.

In the present study, the diffusion bonding of a Ti_3Al-based alloy to a Ni-based superalloy (GH536) was attempted using Ni foil and a newly designed TiNiNb alloy as interlayer. The microstructure and mechanical properties of the joints were investigated. This research work is conducted for the purpose of offering some understanding to the metallurgical behavior at the interface and joint property data for the dissimilar joint.

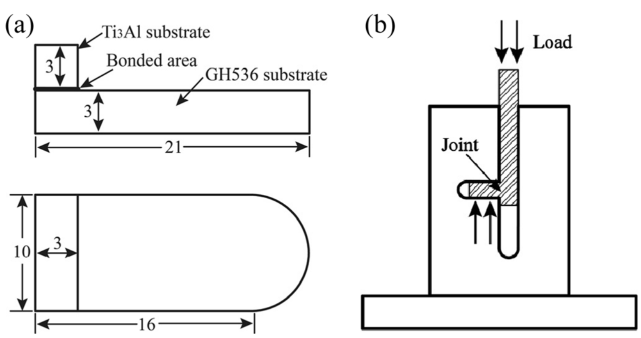

Fig. 1 Illustration of shear test for bonded joints. **a** Geometry of shear test sample in mm. **b** Shear test setup

2 Experimental procedures

The Ti_3Al-based alloy used in this experiment was Ti–24Al–15Nb–1Mo (at.%) alloy which was composed of α_2-Ti_3Al, O-Ti_2AlNb, and β/B2 phases. It was prepared by the following steps: vacuum-consumable electrode arc melting, breaking down in the β/B2 phase fields, forging and rolling in the α_2 + B2 phase field, and heat treating at 980 °C for 1 h followed by cooling in air. The other base material to be joined was GH536 superalloy with a long-term service temperature of 900 °C, whose chemical composition was given in Table 1. Ni foil with a thickness of 15 μm was laminated to double layers in the subsequent bonding experiment. A Ti–(33–43)Ni–(16–25)Nb (wt.%) alloy was designed, aimed at forming a gradient layer between the two base metals. The TiNiNb alloy was firstly cut to sheets with a thickness of 200 μm and then ground to about 50 and 100 μm, respectively.

Prior to bonding, the joined samples, Ni foil and TiNiNb interlayer were ultrasonically cleaned in acetone. During the bonding experiment, the vacuum was kept between 7×10^{-3} Pa and 8×10^{-4} Pa and the heating rate was 10 °C/min. For the Ni foil, the joined couple was heated to a bonding temperature varying from 900 to 1010 °C, with a constant bonding time of 20 min and a fixed pressure of 20 MPa. Concerning TiNiNb interlayer, two dwell times of 10 and 30 min were chosen, and the bonding temperature and pressure were fixed at 980 °C and 20 MPa, respectively. After the

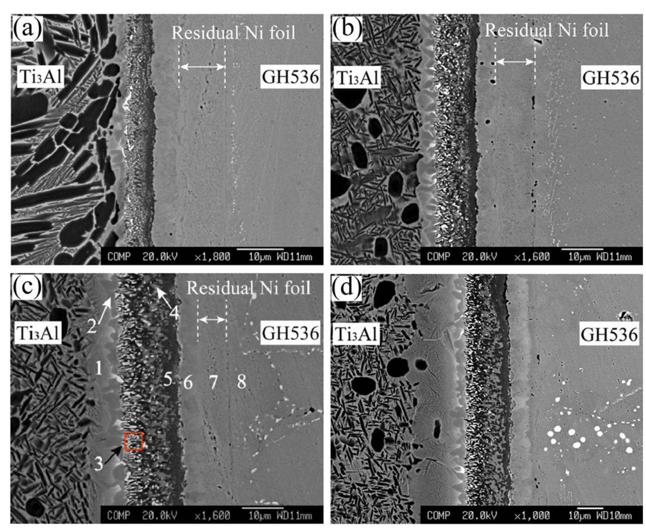

Fig. 2 Backscattered electron images of Ti_3Al/GH536 joints diffusion bonded with Ni foil at (20 MPa/20 min). **a** 900 °C. **b** 940 °C. **c** 980 °C; **d** 1010 °C

Table 2 EPMA analysis results for the microzones in Fig. 2c (at.%)

Microzones	Ti	Al	Nb	Ni	Mo	Fe	Cr	Deduced phases
1	56.318	20.413	16.680	4.376	2.213	/	/	O–Ti_2AlNb
2	43.918	17.365	12.031	25.912	0.774	/	/	$Ti_2Ni(Al,Nb)$
3	28.233	15.611	12.283	42.312	1.561	/	/	$Ni_2Ti(Al,Nb)$
4	36.934	6.849	4.682	50.686	0.636	0.127	0.086	Ni_2Ti
5	31.837	16.862	2.905	48.055	0.124	0.144	0.073	$AlNi_2Ti$ + NiTi
6	21.302	0.747	2.565	74.902	0.025	0.258	0.201	Ni_3Ti
7	1.601	0.092	0.212	92.051	0.495	2.370	3.179	Residual Ni foil
8	0.014	/	/	50.780	4.399	19.645	25.162	GH536 substrate

bonding experiment, the joint was cooled down to 500 °C with a rate of 5 °C/min and then followed by furnace cooling.

The mechanical properties of the bonded samples were assessed by conducting shear tests as schematically shown in Fig. 1. The shear test was measured at room temperature and 600 °C, respectively. The reported average strength was obtained from at least three joints. Joint microstructures and cross-sections of the joints subjected to shear test were examined using a scanning electron microscope (SEM) equipped with an electron probe micro-analyzer (EPMA). Furthermore, the fractured surfaces were also analyzed using an X-ray diffraction (XRD) spectrometer.

3 Results and discussion

3.1 Ti_3Al/GH536 joints diffusion bonded with Ni foil

Figure 2 shows the backscattered electron images (BEIs) of Ti_3Al/GH536 joints diffusion bonded with Ni foil. A tight contact was achieved and the interfacial region was free of common defects. Adjacent to GH536 substrate, Ni foil was retained. Conversely, Ni foil reacted with Ti_3Al substrate, and several reaction layers were formed. Due to reaction and diffusion between Ni foil and Ti_3Al base metal, the total thickness of reaction layers adjacent to Ti_3Al substrate was increased and that of residual Ni foil was decreased with the increase of bonding temperature. For instance, when the bonding experiment was conducted at 900 °C, the total thickness of reaction layers was about 12 μm and that of the residual Ni foil was 10 μm approximately. As bonding temperature increased to 980 °C, the thickness of the former was 27 μm and that of the latter was just 5 μm. No residual Ni foil was visible within the joint bonded at 1010 °C and the thickness of the joint was about 48 μm.

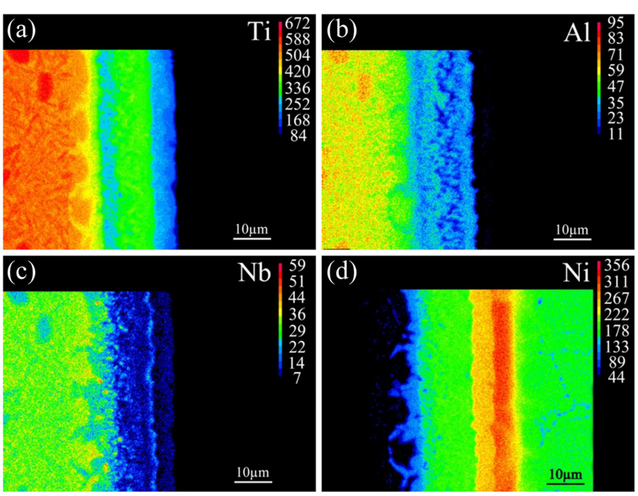

Fig. 3 Element area distribution maps of **a** Ti, **b** Al, **c** Nb, and **d** Ni in Fig. 2c

EPMA analysis results for the typical microzones in Fig. 2c were listed in Table 2. Phase in microzone "1" was O–Ti_2AlNb. Due to diffusion effect, a little amount of element Ni were detected. With the increase of distance from Ti_3Al base metal, the contents of elements Ti, Al, and Nb were decreased and that of Ni was increased as shown in Fig. 3. In microzone "2", the content of Ni was even close to 26 at.%, and the phase could be identified as $Ti_2Ni(Al,Nb)$. In addition, phase in microzones "3" and "4" was Ni_2Ti. It should be noted that about 17 at.% Al was detected in microzone "5", and the phase compositions were deduced to be $AlNi_2Ti$ and NiTi. Microzone "6" was Ni_3Ti phase. The XRD pattern

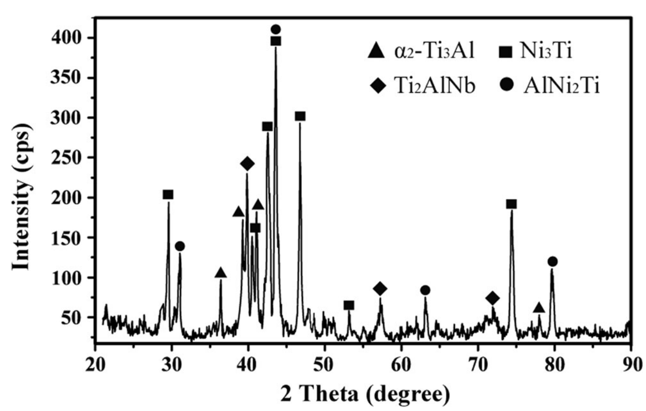

Fig. 4 XRD pattern of the fractured surface for specimen bonded at 980 °C with Ni foil

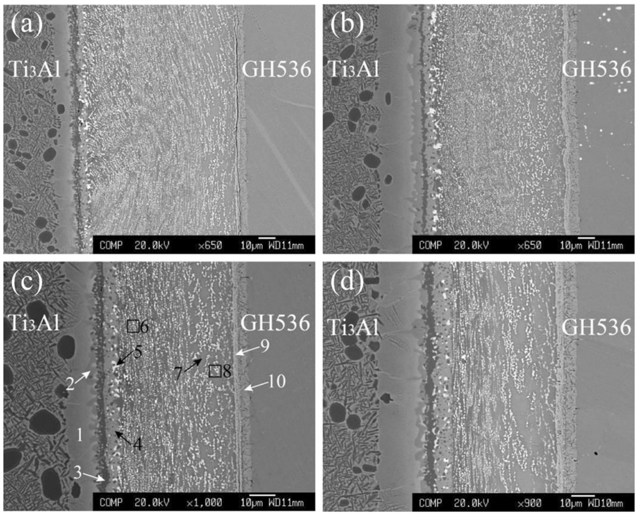

Fig. 5 Backscattered electron images of Ti_3Al/GH536 joints bonded with TiNiNb interlayer at (980 °C/20 MPa). **a** 10 min/100 μm. **b** 30 min/100 μm. **c** 10 min/50 μm. **d** 30 min/50 μm

(Fig. 4) on the as-fractured surface confirms the presence of $AlNi_2Ti$ and Ni_3Ti phases.

Besides, the element area distribution maps in Fig. 3 together with Table 2 signified that only Ti diffused to microzone "6" from Ti_3Al base metal and reacted with Ni foil. Based on Ref. [15], dissolution enthalpies of elements Ti, Al and Nb in melts of Ni were −170, −96, and −143 kJ/mol, respectively. It demonstrated that the affinity between Ti and Ni was stronger than that between Al or Nb with Ni. On the other hand, the content of Ti in Ti_3Al base metal was higher than that of Al and Nb. The diffusion force of Al and Nb was lower than that of Ti. Hence, little Al and Nb were detected, and no Al-Ni or Nb-Ni phases were formed in microzone "6".

For Ti-Ni diffusion couple [16], three reaction layers of Ti_2Ni, TiNi, and Ni_3Ti can be formed in sequence from Ti to Ni, similar to the interfacial structure in this study. The reaction equations of NiTi, $NiTi_2$, and Ni_3Ti were as follows [17]:

$$Ni + Ti \rightarrow TiNi + 67\ \mathrm{kJ}/\mathrm{mol} \quad (1)$$

$$Ni + Ti \rightarrow Ti_2Ni + 83\ \mathrm{kJ}/\mathrm{mol} \quad (2)$$

$$Ni + Ti \rightarrow Ni_3Ti + 140\ \mathrm{kJ}/\mathrm{mol} \quad (3)$$

The formation of Ni_3Ti was more thermodynamically favored than other two phases. Ni_3Ti phase was preferentially precipitated at Ti/Ni interface. Consequently, in the present paper, a Ni_3Ti reaction layer was formed adjacent to residual Ni foil.

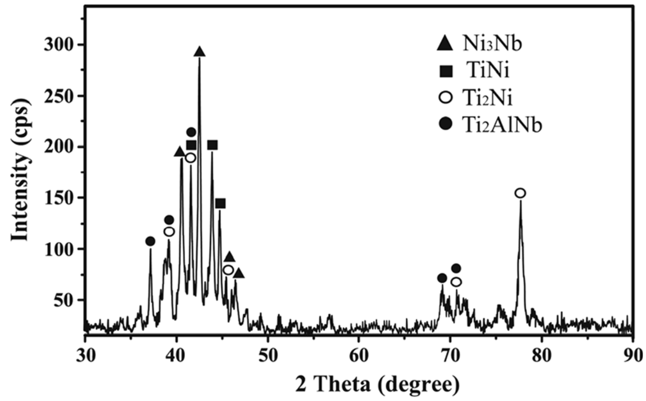

Fig. 6 XRD pattern of the fractured surface for specimen diffusion bonded at 900 °C/20 MPa/20 min with TiNiNb interlayer (50 μm)

3.2 Ti_3Al/GH536 joints diffusion bonded with TiNiNb interlayer

Figure 5 shows the BEIs of Ti_3Al/GH536 joints bonded with TiNiNb interlayer under various bonding conditions. The joints were maintained by gray matrix and white

Table 3 EPMA analysis results for the microzones in Fig. 5c (at.%)

Microzones	Ti	Al	Nb	Ni	Mo	Fe	Cr	Deduced phases
1	57.632	17.061	18.644	4.782	1.881	/	/	O–Ti_2AlNb
2	45.475	15.242	14.351	24.932	/	/	/	Ti_2Ni(Al,Nb)
3	59.521	5.531	2.725	32.233	/	/	/	Ti_2Ni
4	45.254	9.771	16.532	28.433	/	/	/	Ti–Ni–Nb(Al)
5	39.011	4.861	52.862	3.276	/	/	/	(Nb,Ti) solid solution
6	42.181	1.304	17.053	39.462	/	/	/	Ti–Ni–Nb
7	39.874	/	10.001	46.372	/	3.142	0.621	Ti–Ni–Nb
8	35.951	/	15.612	45.944	/	2.081	0.412	Ti–Ni–Nb
9	20.861	/	19.952	21.114	/	19.012	19.071	(Ni,Ti,Nb,Fe,Cr) multi-component phase
10	6.811	/	/	24.974	9.792	18.422	39.341	GH536 substrate dissolved with Ti

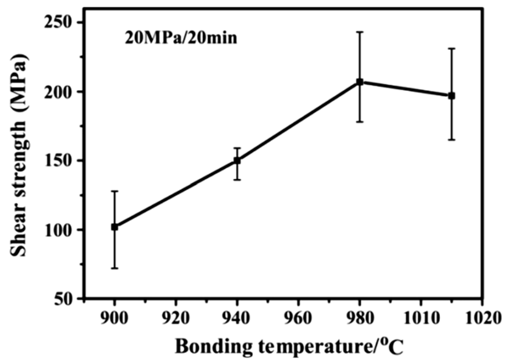

Fig. 7 Effect of bonding temperature on shear strength of Ti_3Al/GH536 joints diffusion bonded with Ni foil

phases. TiNiNb interlayer reacted with base metals and diffusion affected zones (DAZs) were formed. With prolongation of bonding time, the thickness of the DAZ ("9~10") adjacent to GH536 substrate was changed slightly. However, the DAZ ("1~4") adjacent to Ti_3Al substrate was thickened obviously. For example, when the bonding time was 10 min, its thickness was about 20 μm (Fig. 5c). As the bonding time was prolonged to 30 min, the thickness has been increased to 30 μm approximately (Fig. 5d).

Table 3 displays the EPMA analysis results for the typical microzones in Fig. 5c. During bonding process, elements Ti and Al diffused from Ti_3Al base metal to TiNiNb interlayer and on the contrary to Ni atoms due to the concentration gradient. Microzone "1" in Fig. 5c should be the O-Ti_2AlNb phase dissolved with low concentration of Ni. A dark gray phase was visible in microzone "2" and deduced to be Ti_2Ni(Al,Nb). Moreover, a continuous Ti_2Ni reaction layer was formed microzone "3". And the corresponding peaks were confirmed in Fig. 6. Due to the diffusion effect, the content of Ni in microzone "4" was lower than that in the original TiNiNb interlayer.

The content of Ti was higher and Ni was lower for microzone "6" but on the contrary to microzone "8". It might be caused by the diffusion of Ni to Ti_3Al base metal in "6" and that of Ti towards GH536 base metal in "8". The chemical composition in microzone "7" indicated that the content of Nb was lower 50% than that in microzones "6" and "8". It could be deduced that the white phase contained more Nb. It was

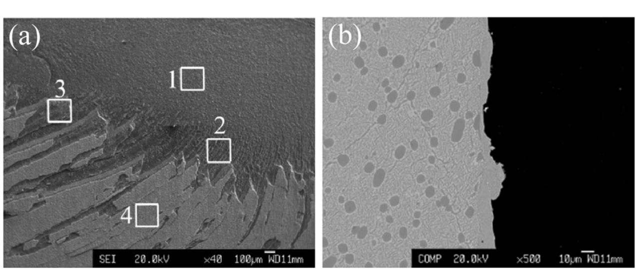

Fig. 8 Fracture surface (Ti_3Al side) (**a**) and cross section (**b**) of the Ti_3Al/GH536 joint diffusion bonded with Ni foil at 980 °C/20 MPa/20 min

Table 4 Compositions of the regions marked by squares in Fig. 8a (at.%)

Microzones	Ti	Al	Nb	Ni	Mo	Deduced phases
1	42.88	14.42	15.75	26.95	/	Ti_2Ni(Al,Nb)
2	43.90	14.83	16.07	22.91	2.29	
3	30.63	14.83	4.54	50.00	/	Ni_2Ti(Al)
4	19.23	4.27	3.87	72.63	/	Ni_3Ti

also confirmed by the composition analysis results in microzone "5". In microzone "1", about 18 at.% Nb was detected, implying the low diffusion force of Nb from TiNiNb interlayer to microzone "1". However, the diffusion force of Ni was high, resulting in the rich of Nb in microzone "5". Microzones "6", "7", and "8" could be identified as residual TiNiNb interlayer. In other words, the joint was maintained by the residual TiNiNb interlayer.

In microzone "9", about 21 at.% Ti diffused to this region and a (Ni,Ti,Nb,Fe,Cr) multi-component phase was formed. Microzones "9" and "10" were identified as diffusion affected zone (DAZ). In general, only little Ti-Ni phases were formed in Ti_3Al/GH536 joints. TiNiNb interlayer suppressed the reaction of Ti and Ni diffused from base metals and played a gradient layer role in composition.

3.3 Mechanical properties

Figure 7 displayed the effect of bonding temperature on room-temperature shear strength of Ti_3Al/GH536 joints diffusion bonded with Ni foil. The joints bonded at 900 and 940 °C showed low shear strengths. With the increase of bonding temperature, the joint strength was improved. The maximum shear strength of 207 MPa was achieved for the joints bonded at 980 °C. Compared with directed diffusion bonded Ti_3Al/GH536 joints (132 MPa), the strength has been increased

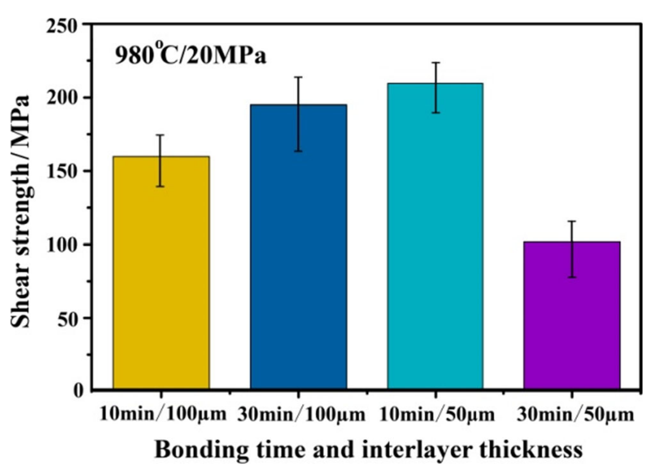

Fig. 9 Average room-temperature shear strength of diffusion bonded Ti_3Al/GH536 joints with TiNiNb interlayer

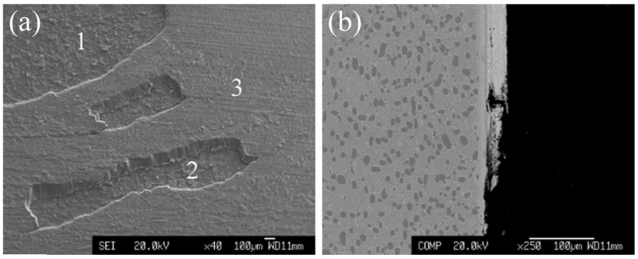

Fig. 10 Fracture surface (Ti_3Al side) (**a**) and cross section (**b**) of the Ti_3Al/GH536 joint bonded at 900 °C/10 min/20 MPa with TiNiNb interlayer (50 μm)

about 58%. The residual Ni foil with a thickness of about 5 μm was ductile and could relax the thermal stress caused by the different thermal expansion coefficients between the two base metals. Hence, the joint strength was relatively increased. However, when the bonding temperature was further increased to 1010 °C, the joint strength decreased slightly. In addition, according to the measured results at high temperature for the joints bonded at 980 °C, the average shear strength at 600 °C was 180 MPa, indicating up to 87% of the room-temperature strength could be maintained. It might be relative to O-Ti_2AlNb and Ti-Ni phases with high temperature stability.

In order to identify the fracture mechanism of the Ti_3Al/GH536 joints, the specimens after shear tests were inspected. As shown in Fig. 8a, the Ti_3Al/Ni/GH536 joint mainly fractured two regions. The composition analysis results at the fractured surface were listed in Table 4. It is easy to notice that the mainly fracture locations were Ti_2Ni(Al,Nb) and Ni_3Ti areas. In fact, Ti_2Ni and Ni_3Ti were brittle compounds with a high hardness of 700 HV [18] and 635 HV [19], respectively. The two compounds, especially Ni_3Ti with a continuous distribution characterization, would increase the joint brittleness and limit the joint strength.

With regard to TiNiNb interlayer, the room-temperature shear strengths of Ti_3Al/GH536 joints were shown in Fig. 9. When the thickness of interlayer was 100 μm, the prolongation of bonding time was beneficial to the joint strength. Nevertheless, prolonging the bonding time caused the decrease of joint strength for the interlayer with a thickness of 50 μm. The maximum shear strength was 209 MPa obtained at 980 °C/10 min/20 MPa, close to that obtained by Ni foil. However, the joint strength at 600 °C was 139 MPa, apparently lower than that achieved through Ni foil. As mentioned above, the Ti_3Al/GH536 joints were maintained by residual TiNiNb interlayer (Fig. 5). Hence, the joint strength was depended on properties of TiNiNb interlayer. Based on the investigation in Ref. [20], the tensile strength of TiNiNb alloy at 600 °C (260 MPa) was only 31% of the room-temperature strength. Consequently, in this study, the shear strength of Ti_3Al/TiNiNb/GH536 joint at 600 °C was obvious lower than that at room-temperature.

Figure 10 displayed the fracture surface and cross section (Ti_3Al side) of the Ti_3Al/TiNiNb/GH536 joint subjected to room-temperature shear test. According to the EDS analysis results presented in Table 5, the chemical compositions of different areas at the fractured surface (Fig. 10a) were very close to those of the Ti_2Ni(Al,Nb) and (Ni,Ti,Nb,Fe,Cr) multi-component phase shown in Fig. 5c. Figure 10b further confirmed the fracture locations. As mentioned above, Ti_2Ni intermetallic compound had a high hardness value (700 HV [18]). Thus, the continuous Ti_2Ni reaction layer was easy to lead to stress concentration and deteriorated the joint properties. Moreover, the micro-cracks existed in microzone “10” (Fig. 5c) severely limited the joint strength and caused the joint mainly fractured along the (Ni,Ti,Nb,Fe,Cr) multi-component phase. This signifies that excessive diffusion of element Ti into GH536 substrate was deleterious to the joint properties.

4 Conclusions

Diffusion bonding between Ti_3Al-based alloy and Ni-based superalloy (GH536) has been successfully achieved using Ni foil and TiNiNb interlayer. Microstructures and mechanical properties of the joints have been investigated. Primary conclusions are summarized as the follows:

As Ni foil was used, it reacted with Ti_3Al-based alloy. Phases Ni_2Ti, $AlNi_2Ti$, and Ni_3Ti were formed due to the strong affinity between elements Ti and Ni. The room-temperature shear strength of the Ti_3Al/GH536 joint bonded at 900 °C/20 MPa/20 min with Ni foil was 207 MPa. Ni-Ti phases limited the joint strength.

For the joint bonded with TiNiNb interlayer, only little Ti-Ni phases were formed, and the reaction of Ti and Ni diffused from base metals was suppressed. The room-temperature strength value of the joint was close to that bonded with Ni foil. The (Ni,Ti,Nb,Fe,Cr) multi-component phase formed at TiNiNb/GH536 interface was the new weak link of the joint.

Table 5 Compositions of the regions marked by squares in Fig. 10a (at.%)

Microzones	Ti	Al	Nb	Ni	Fe	Cr	Mo	Deduced phases
1	53.60	7.86	10.29	28.26	/	/	/	Ti_2Ni(Nb,Al)
2	52.05	7.37	11.74	28.83	/	/	/	
3	26.03	/	17.11	22.88	13.84	16.12	4.01	(Ni,Ti,Nb,Fe,Cr) multi-component phase

Acknowledgements This research work was sponsored by the Aeronautical Science Foundation of China under grant number 03H21009.

References

1. Djanarthany S, Viala JC, Bouix J (2001) An overview of monolithic titanium aluminides based on Ti_3Al and TiAl. Mater Chem Phys 72: 301–319
2. Dimiduk DM, Miracle DB, Ward CH (1992) Development of intermetallic materials for aerospace systems. Mater Sci Technol 8: 367–375
3. Threadgill PL (1995) The prospects for joining titanium aluminides. Mater Sci Eng A 192/193:640–646
4. Xiong HP, Mao JY, Chen BQ, Wang Q, SB W, Li XH (2013) Research advances on the welding and joining technologies of light-mass high-temperature structural materials in aerospace field. J Mater Eng 10:1–12 (in Chinese)
5. Tan LJ, Yao ZK, Zhou W, Guo HZ, Zhao Y (2010) Microstructure and properties of electron beam welded joint of Ti–22Al–25Nb/TC11. Aerosp Sci Technol 14:302–306
6. Chen X, Xie FQ, Ma TJ, Li WY, XQ W (2015) Microstructure evolution and mechanical properties of linear friction welded Ti_2AlNb alloy. J Alloys Compd 646:490–496
7. Cadden CH, Yang NYC, Headley TH (1997) Microstructural evolution and mechanical properties of braze joints in Ti–13.4Al–21.2Nb. Weld J 8:316–325
8. Shiue RK, SK W, Chen YT (2010) Strong bonding of infrared brazed α_2-Ti_3Al and Ti–6Al–4 V using Ti–Cu–Ni fillers. Intermetallics 18:107–114
9. Guo Y, Zhu JM, He ZJ, Lian PF, Wu Q (1996) Diffusion bonding of Ti_3Al base alloy. J Mater Sci Technol 12:467–469
10. Lei ZL, Dong ZJ, Chen YB, Huang L, Zhu RC (2013) Microstructure and mechanical properties of laser welded Ti–22Al–27Nb/TC4 dissimilar alloys. Mater Sci Eng A 559:909–916
11. Chen B, Xiong HP, Mao W, Cheng YY (2010) Microstructures and properties of Ti3Al/Ti3Al and Ti3Al/GH536 joints using Ti–Zr–Cu–Ni brazing filler. J Aeronaut Mater 30(5):35–38 (in Chinese)
12. Chen BQ, Xiong HP, Guo SQ, Sun BB, Chen B, Tang SY (2015) Microstructure and mechanical properties of dissimilar welded Ti_3Al/Ni-based superalloy joint using a Ni–Cu filler alloy. Metall Mater Trans A 46:756–761
13. Chen BQ, Xiong HP, Sun BB, Tang SY, Guo SQ, Zhang XJ (2014) Microstructure evolution and tensile properties of Ti_3Al/Ni-based superalloy welded joint. J Mater Sci Technol 30:715–721
14. Qian JW, Li JL, Hou JB, Xiong JT, Zhang FS, Han ZC (2009) Microstructures and mechanical properties of diffusion bonded Ti2AlNb and GH4169 joints by using Nb + Ni interlayer. J Aeronaut Mater 29(1):57–62 (in Chinese)
15. Miedema AR, Boer FRDE, Boom R, Dorleijn JWF (1977) Model predictions for the enthalpy of formation of transition metal alloys. Calphad 1:341–359
16. Van Dal MJH, Heumeekersm CLP, Kodontsov AA, Van Loo FJJ (2000) Intrinsic diffusion and kirkendall effect in Ni-Pd and Fe-Pd solid solutions. Acta Mater 48:385–396
17. Zhu SL, Yang XJ, DH F, Zhang LY, Li CY, Cui ZD (2005) Stress-strain behavior of porous NiTi alloys prepared by powders sintering. Mater Sci Eng A 408(12):264–268
18. Hiraga H, Inoue T, Shimura H, Matsunawa A (1999) Cavitation erosion mechanism of NiTi coatings made by laser plasma hybrid spraying. Wear 231:272–278
19. Ye LL, Liu ZG, Raviprasad K, Quan MX, Umemoto M, ZQ H (1998) Consolidation of MA amorphous NiTi powders by spark plasma sintering. Mater Sci Eng A 241:290–293
20. Chen BQ, Xiong HP, Sun BB, BR D, Wei ZW, Chen B (2015) Dissimilar joining of Ti_3Al-based alloy to Ni-based superalloy by arc welding technology using gradient filler alloys. Mater Des 87: 732–741